Events Evaluating the Deterioration Risk of Cultural Heritage Building by CFD Simulation—A Case Study of Chaotian Temple in Taiwan

Chia-Yu Liao[1], Meng-Chieh Jeffrey Lee[2], Y.L. Tsai [3]
[1] National Taichung University of Science and Technology, Taiwan - Nicole92630@gmail.com
[2] National Taichung University of Science and Technology, Taiwan - MCJL@nutc.edu.tw
[3] Bureau of Cultural Heritage, Ministry of Culture, Taichung, Taiwan - ch0215@boch.gov.tw

Keywords: Preventive Monitoring, CFD-assisted Diagnostics, Microclimatic RH Variation, H-BIM Modeling, Deterioration-prone Zone Analysis

Abstract

As climate change and urbanization intensify, heritage buildings are increasingly exposed to both environmental and anthropogenic stressors, making their preservation more complex and costly. This study presents an integrated approach that combines Computational Fluid Dynamics (CFD) simulations, Heritage Building Information Modeling (H-BIM), and microclimate monitoring, enhanced by statistical analysis, to assess deterioration risks in historic structures.
By establishing optimized monitoring intervals and evaluating environmental variability, we assess the potential to reduce sensor density without compromising data fidelity. Real-time observations are paired with predictive modeling to identify vulnerable zones early on. Our findings indicate that data-driven preventive monitoring, supported by advanced simulations, offers a practical and scalable strategy for reducing long-term deterioration and enhancing conservation planning.

1. Introduction

The preservation of historic buildings in rapidly urbanizing and climatically unstable regions has become increasingly reliant on digital tools and data-driven strategies. Traditional conservation approaches, which often emphasized post-damage interventions, are now being supplemented or replaced by predictive monitoring and simulation-informed diagnostics. As physical artifacts of collective memory and cultural continuity, heritage structures face diverse stressors from environmental fluctuations and human activities, especially in dense urban contexts where ambient conditions are altered by surrounding infrastructure.

In humid subtropical monsoon climates like Taiwan, historic buildings are particularly susceptible to thermal and hygric instability. The combination of high humidity, seasonal typhoons, and abrupt temperature shifts creates microclimatic environments where moisture retention and airflow stagnation can accelerate material degradation. Architectural components such as timber columns, painted brackets, and carved beams are frequently exposed to repeated cycles of expansion, contraction, and biological colonization. While these risks are well-recognized, practical methods for early detection and scalable intervention remain underdeveloped.

This study proposes a multi-layered framework that integrates Computational Fluid Dynamics (CFD), Heritage Building Information Modeling (H-BIM), and multilevel microclimate monitoring, enhanced with time-series data reconstruction via ARIMA and LSTM models. Rather than focusing solely on identifying existing damage zones, the framework emphasizes the predictive characterization of deterioration-prone microenvironments under varying wind and humidity regimes. The Chaotian Temple in Beigang, Taiwan, serves as the test site, offering a complex architectural and climatic context suitable for multiscale airflow and hygrothermal analysis.

Key research objectives include: (1) identifying spatial zones of environmental stress using CFD-validated airflow profiles, (2) evaluating the influence of vertical microclimatic gradients on material vulnerability, (3) validating predictive accuracy of statistical imputation models for incomplete environmental datasets, and (4) proposing an optimized sensor deployment strategy that minimizes redundancy without compromising data reliability.

The overarching goal is to advance a scalable, simulation-informed conservation approach that aligns environmental diagnostics with resource-efficient monitoring strategies. The outcomes are intended to inform both site-specific interventions at Chaotian Temple and broader applications in preventive heritage management under comparable climatic and urban constraints.

2. Methodology

This study adopts a layered diagnostic framework comprising: (1) microclimate monitoring and statistical reconstruction, and (2) simulation-based environmental verification. The proposed approach is specifically designed to evaluate deterioration risk factors in semi-enclosed temple architecture under urban climatic pressure, using Chaotian Temple in Beigang, Taiwan, as a pilot case. The methodology emphasizes not only the diagnosis of risk zones but also the optimization of monitoring resource allocation through data-informed modeling.

2.1 Physical Monitoring and Data Reconstruction

To capture the dynamics of vertical microclimatic variations, environmental sensors were strategically installed both inside and around the temple, covering representative locations such as the main courtyard, worship halls, and inner atriums. The sensor nodes recorded temperature, relative humidity (RH), wind speed, and wind direction at five-minute intervals for a period exceeding one year. These nodes were distributed across three key spatial layers: the human activity layer, the mid-height architectural zone, and the upper ventilation zone.
Due to Chaotian Temple's architectural configuration—featuring enclosed courtyards, deep eaves, and multi-tiered rooftops—conditions such as thermal stratification and humidity pooling were expected to develop, particularly during southeast monsoon periods, increasing the risk of material degradation.

During the monitoring campaign, sensor outages occasionally caused data gaps. To ensure data continuity, a two-tier imputation framework was developed. For short-term gaps (under 12 hours), an ARIMA(1,0,1) model was applied, selected via Akaike Information Criterion (AIC) and validated using a rolling window cross-validation scheme to ensure temporal stability. For longer-term gaps (over 12 hours), a three-layer Long Short-Term Memory (LSTM) neural network with 64–128–64 recurrent units was used. The network was trained on a 180-day backward window and validated against withheld data segments.

After imputation, the Mean Absolute Percentage Error (MAPE) was 5.4% for temperature and 7.8% for RH, indicating sufficiently high accuracy for use in boundary condition inputs in subsequent simulations.

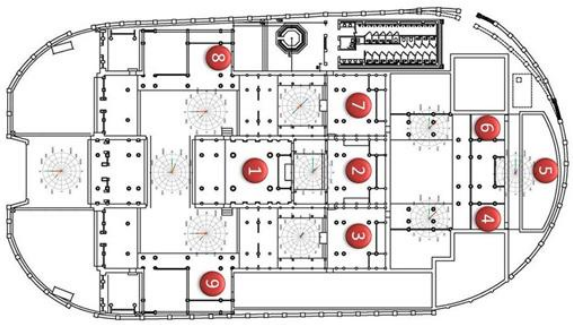

Figure 1 Preliminary Monitoring Allocation Map of Chaotian Temple, Beigang.

2.2 Simulation and Model Validation

To develop a geometrically accurate simulation model, high-resolution mobile LiDAR scanning was performed, capturing point cloud data of the temple and its surrounding 300-meter radius. Over 500 million points were processed in CloudCompare to filter noise and segment geometries. The cleaned dataset was then transformed into a parametric Heritage Building Information Model (H-BIM) using Autodesk Revit, which retained material properties, component connections, and spatial boundaries necessary for airflow analysis.

In the simulation phase, a three-dimensional CFD model was constructed in ANSYS Fluent. The domain was meshed using unstructured tetrahedral elements, with inflation layers added along building surfaces to enhance vortex and shear layer resolution. The minimum mesh size was set to 5 mm to resolve small-scale turbulence structures. Boundary conditions were defined using a steady-state inflow at 10 m/s, with wind directions set based on long-term meteorological data—namely, prevailing north (N), north-northeast (NNE), and northeast (NE) winds.

To balance simulation precision and computational efficiency, the standard k-ε turbulence model was employed, known for its robustness in architectural ventilation simulations.

To analyze vertical airflow characteristics and inter-layer interactions, three representative horizontal slices were defined at 2.2 m (breathing zone), 5 m (mid-structure), and 20 m (roof level). Simulated parameters—including wind speed, pressure, and vorticity—were extracted and compared point-by-point against in situ measurements. Validation results yielded an R^2 of 0.89 and a MAPE of 9.6%, confirming the reliability of the CFD model and supporting its use for deterioration risk indexing.

2.3 Risk Mapping and Conservation Strategy

By integrating empirical measurements with CFD simulation outputs, a Cultural Heritage Degradation Risk Index was developed. This index synthesizes key environmental indicators such as vertical RH gradients, airflow stagnation zones, abnormal wind pressure regions, and thermal accumulation hotspots. The index was visualized via a GIS-based mapping interface, overlaid with CFD-generated airflow vectors and isobaric pressure contours to illustrate spatial patterns of long-term environmental stress.

To improve sensor deployment efficiency, a sensor optimization model was implemented. Twenty alternative deployment schemes were simulated, with sensitivity analysis and diagnostic accuracy tests conducted for each. The results showed that a 32% reduction in sensor count could still preserve over 90% of deterioration detection accuracy.
Three practical outputs were generated:
Zonal sensor deployment guidelines, facilitating future expansion to similar heritage sites;

Calibrated regression curves between RH and ΔT, supporting anomaly detection and microclimate modeling;

A data-driven early warning system and predictive maintenance schedule, aimed at improving the precision and operational efficiency of conservation practices.

Taken together, these methods resulted in the successful construction of a deterioration risk index and spatial mapping system. The proposed framework offers a quantitative basis for sensor placement, anomaly detection, and preventive maintenance planning in heritage environments.

3. CFD Simulation

To simulate the intricate airflow dynamics around and within the temple, we conducted unsteady-state simulations using the k-ε turbulence model. The modeled domain included the main hall, surrounding dormitories, enclosing walls, and nearby structures. Boundary conditions were defined based on local meteorological data, focusing on dominant wind directions from the north (N, NNE, NE) at 10 m/s.

Airflow behavior was analyzed across three vertical sections (2.2 m, 5 m, and 20 m). At lower levels, vortex stagnation zones formed due to surface friction and structural obstructions. At mid-elevation (5 m), airflow became more stable, yet localized eddies were observed near painted facades, suggesting areas prone to moisture retention.

In scenarios involving partial openings—particularly B-type configurations—internal backflow was detected, potentially increasing the risk of latent moisture damage.
These findings informed the subsequent microclimate analysis and risk mapping.

In this study, ANSYS Fluent was employed as the primary platform for performing Computational Fluid Dynamics (CFD) simulations aimed at investigating the potential deterioration risks associated with airflow and moisture distribution at Chaotian Temple. The simulations were designed to analyze

both indoor and outdoor airflow patterns and to identify spatiotemporal hotspots of humidity accumulation that could contribute to material degradation. Additionally, airflow interaction under different architectural opening configurations was examined to evaluate internal ventilation dynamics.

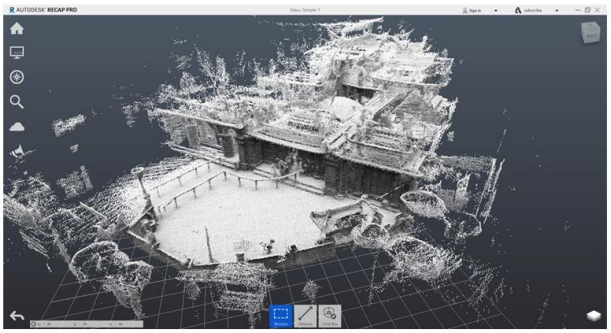

Figure 2 Laser-Scanned Point Cloud of Chaotian Temple as a 3D Reference Model

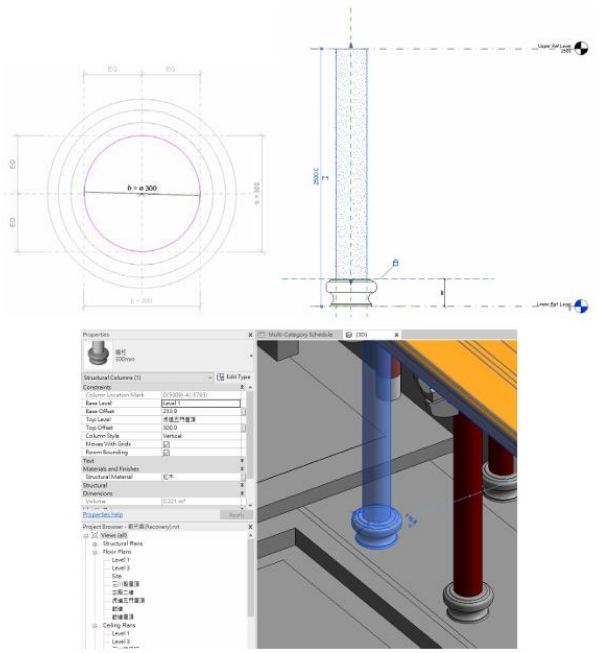

Figure 3 Dimensional and Quantitative Data of Chaotian Temple’s Architectural Components

We began by constructing a detailed three-dimensional geometric model of the temple complex using Heritage Building Information Modeling (H-BIM), incorporating surrounding elements such as the main temple structure, pilgrim dormitory, perimeter walls, and elevated roadways. This model was exported in high-resolution STL format and imported into the CFD preprocessing stage. An unstructured mesh was generated using ANSYS Meshing, with fine-grained meshing near critical boundary areas such as walls, openings, and eaves. The minimum cell size in these localized regions was set to less than 0.01 meters, ensuring high-resolution simulation of microscale airflow behavior along architectural surfaces.

Figure 4 Massing Model of the Building Created Using 3D Modeling Software

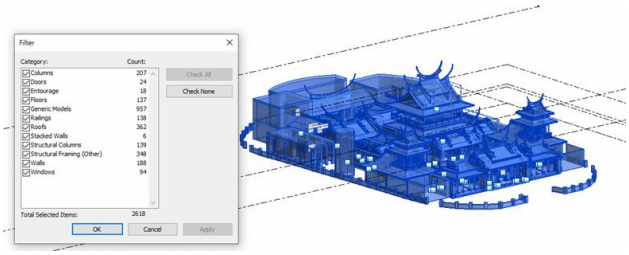

Figure 5 Quantitative Data of Architectural Elements at Chaotian Temple, Beigang

An unsteady flow design was adopted to capture real-world temporal variations in wind conditions. Simulations utilized the standard k-ε turbulence model, chosen for its computational efficiency and robust performance in predicting turbulent flow in enclosed and semi-enclosed environments. Boundary conditions included a velocity-inlet at the windward boundary, a pressure-outlet at the leeward boundary, and no-slip wall conditions applied to all ground and surface elements.

Wind profiles were defined based on meteorological statistics from the Central Weather Bureau, focusing on three dominant wind directions—North (23.8%), North-Northeast (22.4%), and Northeast (4.6%)—each assigned a uniform inflow speed of 10 m/s to simulate their effects on ventilation and moisture transport across the temple layout.

To capture vertical variations in airflow, velocity and pressure fields were extracted at three elevation slices: 2.2 m, 5 m, and 20 m, corresponding to critical occupant and structural levels. Results revealed prominent vortex stagnation zones near ground level due to surface roughness and architectural shielding, where airflow slowed and eddies formed. These areas coincided with zones of observed high humidity accumulation, with moisture levels averaging 12.7% higher than in adjacent open-air sections. Although airflow became more stable at the 5 m elevation, localized eddies persisted near the painted facade of the front hall, suggesting potential zones for moisture entrapment and longer retention times.

Further, we modeled three opening configuration scenarios to evaluate their impact on internal air circulation and humidity dynamics:
Scenario A: fully open structure
Scenario B: partially open (e.g., traditional three-bay front hall)
Scenario C: fully enclosed layout
Among these, Scenario B exhibited the highest turbulence intensity and internal recirculation. Notably, the three-bay vestibule design induced significant backflow near the central

sanctum, due to sidewall-guided airflow redirection, impeding moisture evacuation and creating persistent humid microenvironments—conditions that elevate the risk of material deterioration over time.

To verify the validity of the simulation, we cross-referenced the CFD output—specifically air velocity, pressure distribution, and relative humidity contours—with field measurements obtained from microclimate sensors. The Mean Absolute Percentage Error (MAPE) was approximately 9.4%, and the coefficient of determination (R^2) reached 0.89, indicating a high level of accuracy and predictive reliability.

These results affirm that CFD simulation is a powerful diagnostic tool for identifying and mitigating airflow-related risks in complex heritage environments. The approach provides actionable insights to inform preventive conservation strategies and ventilation optimization tailored to site-specific microclimatic behaviors.

4. Discussion

The CFD simulation outputs revealed layered wind behavior across distinct vertical planes, prompting a refined analysis of airflow-driven microclimatic conditions in semi-enclosed heritage spaces. In particular, wind deflection caused by high-rise structures proximal to Chaotian Temple produced low-velocity vortex zones at pedestrian height, which align spatially with areas known to exhibit prolonged moisture retention and biological growth. While CFD results captured transient eddy formation and pressure stagnation zones, their true conservation value emerged when overlaid with high-frequency RH and temperature records from on-site sensors. Regions exhibiting persistent $\Delta T/\Delta RH$ divergence patterns were further validated via in-person field inspections, confirming discoloration, surface flaking, and localized mold colonization. This convergence of modeled turbulence behavior and empirical degradation markers enabled the construction of a robust deterioration risk index.

Boundary conditions for the simulations were defined using multi-year statistical wind data from the Central Weather Bureau, reflecting dominant inflows from the north and northeast quadrants. Simulated airflow fields at different height slices demonstrated that architectural shielding by dormitories and wall corridors significantly modified local wind trajectories, deviating them from broader-scale meteorological expectations. The vertical airflow structure showed vapor stagnation near ground level, rotational shear at mid-elevation, and relatively undisturbed flow at roof level, highlighting the complex layering effects present in traditional courtyard-style architecture.

To further support preventive conservation, a dual-path statistical prediction model was implemented. ARIMA was applied to reconstruct short-term sensor data gaps, while a recurrent LSTM network provided accurate long-range forecasts of RH and temperature shifts. These predictive results informed the development of a sensor optimization matrix, which evaluated environmental coverage across 20 deployment permutations. The final configuration achieved over 90% zone fidelity while reducing physical sensor count by approximately 30%, demonstrating a resource-efficient strategy for long-term monitoring.

Finally, the integration of high-resolution 3D scanning and H-BIM modeling enabled deterioration indicators to be spatially anchored and tagged across structural elements. Each component was assigned a vulnerability profile based on material type, exposure orientation, and RH fluctuation severity. This parameterized BIM environment supports targeted restoration, automated risk tracking, and scalable conservation planning for other similarly configured heritage structures.

Figure 6 Overlay of Chaotian Temple Architectural Plan and Laser-Scanned Point Cloud

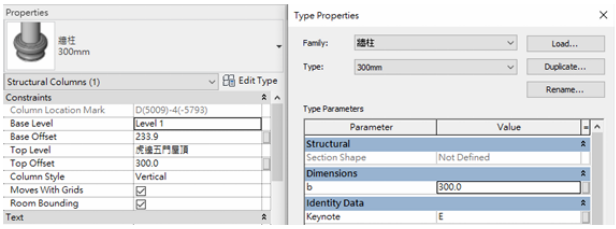

Figure 7 Dimensional and Parametric Data of the Chaotian Temple BIM Model

5. Conclusion

This study illustrates the benefits of a multi-layered strategy for preventive conservation, integrating empirical monitoring, predictive analytics, and CFD-based simulations. The simulated moisture-prone zones closely aligned with observed deterioration, affirming the robustness of the proposed methodology.

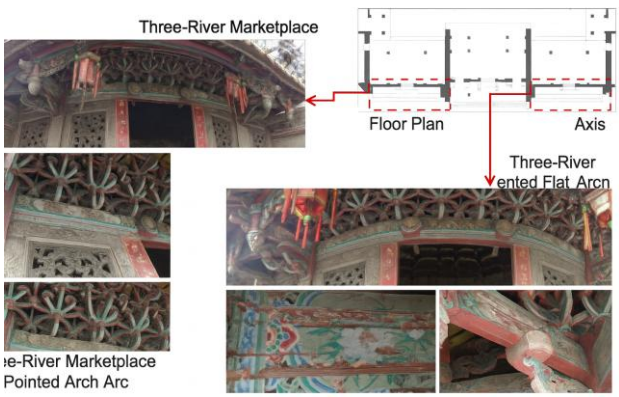

Figure 8 Damage to Sanchuan Hall's Decorative Paintings Caused by Wind Disturbances from Adjacent Buildings

This study conducted statistical analysis on temperature (T) and relative humidity (RH) data collected from microclimate monitoring stations installed in the Sanchuan Hall and Guanyin Hall of Chaotian Temple. The aim was to evaluate

the seasonal stability of indoor microclimatic conditions.

Due to the semi-enclosed nature of these interior spaces and the presence of vertical thermal stratification, it was found that placing a single sensor at both upper and lower levels within each hall was sufficient. The temperature difference between these two levels (ΔT) demonstrated a consistent linear correlation with the corresponding difference in relative humidity (ΔRH), enabling the estimation of RH variation based solely on ΔT.

This relationship provides a reliable basis for simplifying sensor deployment while maintaining effective microclimate monitoring in heritage buildings with vertically layered thermal behavior.

Linear Regression Formulas:

1. Slope Formula:

$m = \Sigma(x - \bar{x})(y - \bar{y}) / \Sigma(x - \bar{x})^2$ (Equation 1-1)

2. Intercept Formula:

$b = \bar{y} - m \cdot \bar{x}$ (Equation 1-2)

Where:;

$\bar{x}$ and $\bar{y}$ are the sample means of x and y, respectively. Σ represents the summation over all sample data.
m is the slope of the regression line.
b is the y-intercept of the regression

line. A simplified regression model:

$\Delta RH = \alpha \times \Delta T + \beta$ (Equation 2)

In this analysis, ΔRH represents the relative humidity difference between upper and lower levels, while ΔT denotes the corresponding temperature difference. The regression coefficients α and β were derived from empirical data, and the coefficient of determination (R^2) was calculated for each season to assess the predictive strength and microclimatic stability of the observed spaces.

The seasonal regression results for both Sanchuan Hall and Guanyin Hall are summarized in Table 2 and Table 3, covering data from spring, summer, autumn, and winter in the years 2014 and 2015, respectively.

It is important to note that the accuracy of this analysis depends on the availability of complete and continuous time-series data. To address missing values, this study first employed the ARIMA model to impute short-term data gaps, followed by Long Short-Term Memory (LSTM) neural networks to model longer-term trends. The imputed datasets were then cross- validated against data from nearby Central Weather Bureau stations, showing strong agreement in temporal patterns and confirming the reliability of the reconstructed series.

The seasonal and spatial regression analysis not only produced R^2 values indicative of environmental stability across years and architectural zones, but also offered a quantitative foundation for subsequent risk identification and sensor placement strategies in preventive conservation planning.

Table 2 Temperature and Humidity Variability Across the Halls

Layer/Sensor	Temp (°C) - San Guan	Humidity (%)- anGuan	Temp (°C) - Guanyin	Humidity (%)- Guanyin
UpperSensor1	4.8	15.9	4.7	15.8
UpperSensor2	4.5	18.4	4.6	18.9
UpperSensor3	4.8	16.0	4.0	17.3
UpperSensor4	4.9	19.7	3.8	13.7
UpperAverage	4.8	17.5	4.2	16.4
Lower Layer	4.2	15.7	4.1	16.6

Table 3 Correlation Coefficients of Temperature and Relative Humidity Across Vertical Layers at Chaotian Temple During Winter and Spring

Building	α (Winter)	β (Winter)	R^2 (Winter)	α (Spring)	β (Spring)	R^2 (Spring)
San Guan Hall	-3.78	0.39	0.96	-4.01	1.47	0.94
Guanyin Hall	-2.17	-1.10	0.32	-2.53	1.46	0.96

Table 4 Correlation Coefficients of Temperature and Relative Humidity Across Different Elevations at Chaotian Temple in Summer and Autumn

Building	α (Summer)	β (Summer)	R^2 (Summer)	α (Autumn)	β (Autumn)	R^2 (Autumn)
San Guan Hall	-3.90	0.45	0.95	-2.92	-0.25	0.76
Guanyin Hall	-1.87	-0.56	0.99	-2.80	-0.57	0.76

Table 5 2014 Data for the Two Main Halls

R^2	Spring (2014)	Summer (2014)	Autumn (2014)	Winter (2014)
San Guan Hall	0.9927	0.9367	0.5232	0.4821
Guanyin Hall	0.9868	0.9191	0.3109	0.0171

Table 6 2015 Data for the Two Main Halls

R^2	Spring (2015)	Summer (2015)	Autumn (2015)	Winter (2015)
San Guan Hall	0.8753	0.9075	0.5232	0.9714
Guanyin Hall	0.4038	0.9584	0.3614	0.6178

achieved high predictive accuracy (R^2 approaching 1), suggesting that future monitoring can be streamlined using only one or two strategically placed sensors. This approach significantly reduces the cost and complexity of continuous environmental monitoring while maintaining analytical robustness.

Vertical stratification of airflow characteristics was evident across the monitored elevations. At 2.2 meters—corresponding to pedestrian height—airflow was notably diverted toward the southeast, with ground-level architectural obstructions inducing coherent vortex structures and recirculation zones. These low-level disturbances are indicative of inhibited natural ventilation and increased stagnation potential. At 5 meters, the airflow exhibited elevated turbulence intensity, largely attributable to lateral interference from adjacent built forms, particularly the Cultural Building, which disrupted the laminar profile and promoted unsteady eddy formations.

At the upper elevation of 20 meters, while mean wind velocity stabilized and conformed more closely to prevailing synoptic wind patterns, a pronounced vertical pressure gradient was detected. This gradient poses potential aerodynamic loading risks on exposed structural components, especially at parapets and rooflines.

References

Chan, K.L., Qin K., 2017: Biomass burning related pollution and their contributions to the local air quality in Hong Kong. *Int. Arch. Photogramm. Remote Sens. Spatial Inf. Sci*., XLII-2/W7, 29-36. doi.org/10.5194/isprs-archives-XLII-2-W7-29-2017.

Dubayah, R.O., Swatantran, A., Huang, W., Duncanson, L., Tang, H.,Johnson, K., Dunne, J.O., Hurtt, G.C., 2017. CMS: LiDAR-derived Biomass, Canopy Height and Cover, Sonoma County, California, 2013. ORNL DAAC, Oak Ridge, Tennessee, USA. doi.org/10.3334/ORNLDAAC/1523.

Förstner, W., Wrobel, B., 2016: *Photogrammetric Computer Vision*. Springer Nature, Cham.

Gago-Silva, A., 2016. GRASS GIS in Grid Environment. doi.org/10.6084/m9.figshare.3188950.

GRASS Development Team, 2015. Geographic Resources Analysis Support System (GRASS) Software, Version 6.4. Open Source Geospatial Foundation. grass.osgeo.org (1 June 2017).

GRASS Development Team, 2017. Geographic Resources Analysis Support System (GRASS) Software. Open Source Geospatial Foundation. grass.osgeo.org (20 September 2017).

Lennert, M., GRASS Development Team, 2017. Addon i.segment.stats. Geographic Resources Analysis Support System (GRASS) Software, Version 7.2, Open Source Geospatial Foundation. grass.osgeo.org/grass7/manuals/addons/i.segment.stats (1 June 2017).

Maas, A., Rottensteiner, F., Heipke, C., 2017. Classification under label noise using outdated maps. *ISPRS Ann. Photogramm. Remote Sens. Spatial Inf. Sci.*, IV-1/W1, 215-222. doi.org/10.5194/isprs-annals-IV-1-W1-215-2017.

Michalis, P., Dowman, I., 2008: A Generic Model for Along-Track Stereo Sensors Using Rigorous Orbit Mechanics. *Photogrammetric Engineering & Remote Sensing* 74(3), 303-309.

Smith, J., 1987a. Close range photogrammetry for analyzing distressed trees. *Photogrammetria*, 42(1), 47-56.

Smith, J., 1987b. Economic printing of color orthophotos. Report KRL-01234, Kennedy Research Laboratories, Arlington, VA, USA.

Smith, J., 2000. Remote sensing to predict volcano outbursts. *Int. Arch. Photogramm. Remote Sens. Spatial Inf. Sci.*, XXVII-B1, 456-469.